ELSEVIER

J. Construct. Steel Res. Vol. 44, Nos. 1–2, pp. 23–50, 1997

Printed in Great Britain
PII: S0143-974X(97)00036-9 0143-974X/97 $17.00 + 0.00

Stability and Ductility of Steel Elements

Ioannis Vayas

Department of Civil Engineering, National Technical University of Athens, Patission 42, GR-10682 Athens, Greece

ABSTRACT

This paper presents a method for the simulation of the behaviour of steel structural elements both before and after the attainment of the ultimate load. It is based on a strain-oriented formulation of the governing relations usually applied to stability problems. Accordingly, the response of elements subjected to specific strain conditions is determined. Several types of elements, including single plate panels, transversely loaded beams, axially loaded columns and compressed stiffened plates with imperfections, are investigated. The analytical results are compared with experimental ones. Various modes of failure with different characteristics in the post-critical region are detected. The elements examined show that if bending and plate buckling prevail, the failure mode is ductile, while in the case of global buckling and lateral torsional buckling, a nonductile failure is expected. The method may serve for both stability and ductility evaluations of steel elements, which are needed if the design format includes a direct comparison between ductility supply and ductility demand for structural elements. © 1997 Elsevier Science Ltd.

NOTATION

A	Cross-sectional area
A_e	Area of the effective cross-section
b	Gross width
b_e	Effective width
E	Modulus of elasticity
E_T	Tangent modulus
e	Global imperfection (deflection)
f_y	Yield stress
N_{Sd}	Applied axial load
M_{Sd}	Applied bending moment

t	Plate thickness
W	Section modulus
W_e	Modulus of the effective cross-section
α	Imperfection factor
δ	Midspan deflection
ϵ	Strain
ϵ_y	Yield strain
θ	End rotation
k_σ	Buckling coefficient
$\bar{\lambda}$	Dimensionless slenderness
ν	Poisson's ratio
σ	Stress according to the structural response
σ_0	Stress according to the material law
σ_{cr}	Critical elastic stress
χ	Reduction factor due to buckling

1 INTRODUCTION

The behaviour of steel elements is very much dependent on the type of structure under consideration, the geometric, loading and supporting conditions, the geometrical imperfections, the residual stresses, etc. The element response may be expressed in terms of generalized load–deformation curves, where the term 'load' describes force, moment, stress, etc., while the term 'deformation' describes deflection, rotation, curvature, etc. Analytically predicted load–deformation curves for several elastic structural elements are shown in Fig. 1. The figure shows the differences in response for the different elements

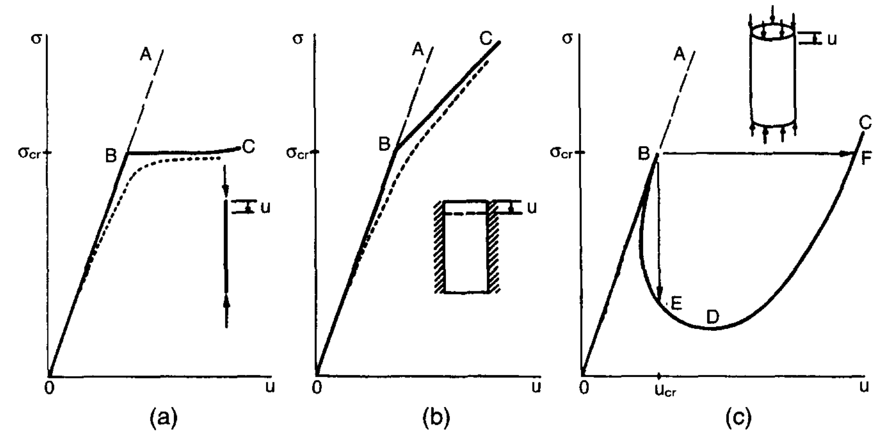

Fig. 1. Analytically predicted elastic response of (a) columns, (b) plates and (c) shells under compression.

under consideration. The behaviour of real steel elements and subassemblages is, however, different from the predicted one corresponding to elastic behaviour. Experimentally derived load–deformation curves of elements that fail due to instability, which constitute the vast majority in steel structures, show that the structural response is qualitatively very much the same (Fig. 2). The load–deformation characteristic consists of a linear part L at small loads, a nonlinear part NL due to geometrical nonlinearities and plasticity, and an unloading part UL after the attainment of the ultimate load. The type of failure is characterized by the unloading part UL of the curve. It is ductile if the rate of unloading is small and nonductile if this rate is large. Accordingly, ductility may be defined as the capacity of an element, member, etc. to exhibit large inelastic deformations without considerable reduction in strength.

Steel is as a material very ductile. It exhibits inelastic deformations several times larger than those at first yield, thereby increasing its strength due to strain hardening. However, the ductility of steel elements or members is adversely influenced by stability loss. These elements fail usually due to several possible instability modes like local, flexural, lateral torsional buckling, etc. These failure modes acting individually or in combination result in reductions of ductility. Accordingly, stability and ductility influence each other very much.

The importance of ductility and the post-ultimate branch of the load–deformation characteristic of a structural element, a subassemblage or a complete structure, was recognized from the early application of steel design codes. Older steel regulations like BS 449 [1] or DIN 1050 [2], were based on strength and defined the end of linearity (point Y in Fig. 2) as the limit state.

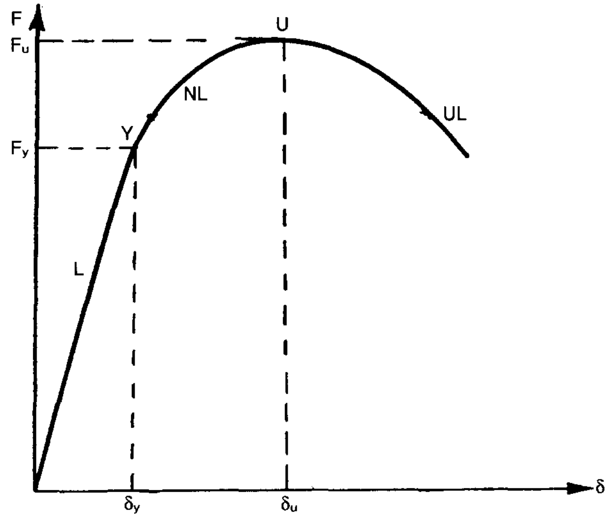

Fig. 2. Response of real steel elements.

This may give the impression that the other parts NL and UL of the structural response were neglected. This impression is wrong however, because in addition to the limit state definition, variable safety factors dependent on the type of failure were introduced. Accordingly, larger values of safety factors were prescribed for nonductile failure modes (or failure without warning) and smaller values for ductile failure modes (or failure with warning). In that way, the parts NL and UL were indirectly taken into account in structural design.

New design regulations, like LRFD [3] or Eurocode 3 [4], rely more directly on ductility. The limit state is now defined as point U of the structural characteristic, so that nonlinearities, part NL of the curve, are directly taken into account. The application of this criterion to a subassemblage (e.g. a portal frame) implies that individual elements have already reached their limit state and they move towards the unloading part UL. In that case it is plastic redistribution that ensures the increase of the total applied load on the structure. This indicates that plastic analysis relies directly on ductility. Ductility is also the basis of design in another important engineering field that deals with the seismic design of steel structures. In both cases an evaluation of the ductility provided by the various members is required.

Design specifications provide rules for the determination of limit 'loads' (stresses, moments, forces) of steel members. Based on observation of actual behaviour in tests and on theoretical considerations, a 'design model' is selected, leading to a strength function. Then, by statistical interpretation of all available test data, the efficiency of the model is checked and appropriate values of the safety factors are evaluated. This leads to the determination of design values of the strength function. Standard procedures for such statistical evaluations are provided by the relevant codes (e.g. Eurocode 3, Annex Z [5]).

After having defined the limit 'load' (Fig. 2, point U), current design regulations provide simple methods for the simulation of the structural behaviour up to this load (Fig. 2, regions L and NL). Unfortunately, there is a lack of relevant simple methods for the description of the structural response beyond the limit load.

This paper presents a method for the simulation of the behaviour of members beyond the ultimate load, thus allowing the evaluation of their ductility. The method may be applied to various members such as plates, beams, columns or beam columns which may fail due to one or more instability modes. The application of the method is shown for both simple and complicated elements and failure modes, its validity is verified by comparison with corresponding experimental results. It will also be shown that for cases where coupled instabilities appear, it is necessary to include all member characteristics in the criteria for classification with respect to ductility.

2 STRAIN-ORIENTED METHOD FOR STABILITY PROBLEMS

Although the governing differential equations may be different, most problems of stability are currently treated in a similar way (Fig. 3). In a first step a dimensionless slenderness is determined from

$$\bar{\lambda} = \sqrt{\frac{f_y}{\sigma_{cr}}} \tag{1}$$

where f_y is the yield stress and σ_{cr} is the critical elastic stress of the element.

The evaluation of a reduction factor χ as a function of the slenderness according to a buckling curve follows. The ultimate stress is finally given by

$$\sigma_u = \chi f_y. \tag{2}$$

The method applies equally to most stability problems. The type of element under consideration (linear element, plate, shell), the buckling mode (local, global buckling, torsional lateral buckling, etc.), the loading and supporting conditions are taken into account by appropriate selection of the critical stress σ_{cr} and the buckling curve.

The methodology described above serves the evaluation of the ultimate stress σ_u (or load F_u). If the entire element characteristic up to the limit point U, Fig. 2, is to be determined, the procedure is modified as follows.

For an applied strain ϵ smaller than the yield strain ϵ_y, the corresponding stress is, according to the material law, equal to

$$\sigma_0 = \epsilon E. \tag{3}$$

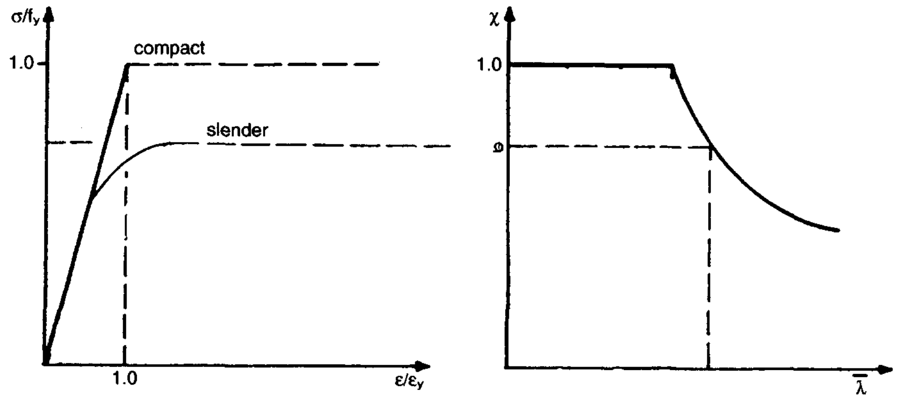

Fig. 3. Treatment of stability problems: (a) stress–strain characteristic; (b) buckling curve.

Eqn (1) is then modified to

$$\bar{\lambda} = \sqrt{\frac{\sigma_0}{\sigma_{cr}}}\ . \tag{4}$$

From this slenderness value, which is lower than that determined by eqn (1), a new reduction factor is determined according to the buckling curve. The element response that corresponds to the strain ϵ is found from

$$\sigma = \chi\sigma_0. \tag{5}$$

Linear behaviour is characterized by $\chi = 1$, while region NL corresponds to values $\chi < 1$.

Eqns (3) and (4) imply that slender elements with small values of σ_{cr} exhibit linear behaviour only at small strain levels, while compact elements may behave linearly up to the yield strain (Fig. 3(a)). The limit stress is, according to this procedure, always achieved at the level of the yield strain.

The main disadvantage of this method which is incorporated in many design codes (Eurocode 3 [4]) is that it simulates the element behaviour only up to the yield strain. For an accurate description of the structural response over the entire range of strain and thus beyond the limit load, a strain-oriented methodology for strains larger than ϵ_y is required. The influence of strain hardening has also to be taken into account, to allow for the evaluation of e.g. resistance moments of beams above the plastic moment M_p.

In the following, a strain-oriented method presented by Vayas and Psycharis [6], allowing for the simulation of the element behaviour beyond failure with inclusion of strain hardening effects, will be shown. The element under consideration is subjected to a strain ϵ. In the case that this strain is lower than the yield strain ϵ_y, the procedure as described above is followed. Accordingly, eqn (4) becomes

$$\bar{\lambda} = \sqrt{\frac{\epsilon E}{\sigma_{cr}}} \tag{6}$$

and eqn (5) is written as

$$\sigma = \chi\epsilon E. \tag{7}$$

In the case where $\epsilon > \epsilon_y$ (Fig. 4), if a bilinear σ–ϵ relationship for steel is assumed, the stress according to the material law is equal to

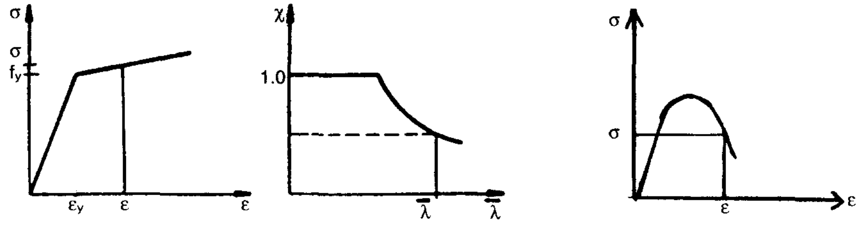

Fig. 4. Strain-oriented methodology: (a) σ–ϵ characteristic; (b) buckling curve; (c) element response.

$$\sigma_0 = [\epsilon_y + (\epsilon - \epsilon_y)E_T/E]E \tag{8}$$

where E and E_T are the modulus of elasticity and the tangent modulus of elasticity of steel.

The slenderness may be determined from

$$\bar{\lambda} = \sqrt{\frac{[\zeta\epsilon_y + \eta(\epsilon - \epsilon_y)]E}{\sigma_{cr}}} \tag{9}$$

where ζ and η are parameters to be determined according to the following considerations.

Eqns (4) and (8) imply that η should be taken equal to E_T/E if $\bar{\lambda}$ is directly connected to the stress, while eqn (6) indicates that $\eta = 1$ if it is directly connected to the strain. These expressions are identical as long as the material behaviour is elastic. This is no longer valid for strains larger than ϵ_y. For such strains it is expected that the value of η is between the two limits of E_T/E and 1 of the elastic region. For its determination, extensive analyses with different expressions for η were carried out. It was shown by Vayas and Psycharis [6] that constant values of $\eta = 0.5$ and $\zeta = 1.0$ lead to results that compare well on average with the corresponding experimental ones. Wittemann [7] suggested the following expressions by comparison with rigid plastic analysis:

$$\epsilon_y < \epsilon \leq 6\epsilon_y\text{: } \zeta = 1.0 \ \eta = 0.5$$

$$6\epsilon_y < \epsilon \leq 20\epsilon_y\text{: } \zeta = 3.5 \ \eta = 0.2$$

$$20\epsilon_y < \epsilon\text{: } \zeta = 6.3 \ \eta = 0.1.$$

In the present work the initially mentioned values of 0.5 and 1.0 for η and ζ will be applied for reasons of simplicity.

Finally, after determination of the reduction factor, the response of the element is given by

$$\sigma = \chi\sigma_0. \tag{10}$$

The above described procedure is adopted in order to analytically predict the response of various structural elements as shown subsequently.

3 BEHAVIOUR OF PLATES

The accurate simulation of the behaviour of an individual plate panel is a cornerstone of the analysis of steel sections, since it constitutes the basic element for more complicated cross-sections. For the analysis of plates, the method of the effective width has proven to be most advantageous. This method works with reduced, 'effective' widths and full stresses rather than with gross widths and reduced stresses. Accordingly, the reduction factor χ as determined by the buckling curve is applied to the gross width b of the plate. An effective width is calculated from

$$b_e = \chi b \tag{11}$$

and the final response of the plate panel is given by

$$\sigma = \frac{b_e}{b}\,\sigma_0. \tag{12}$$

This procedure may be applied to plates subjected to both uniform and linearly varying strain along their edges (Fig. 5). Initially, the effective width

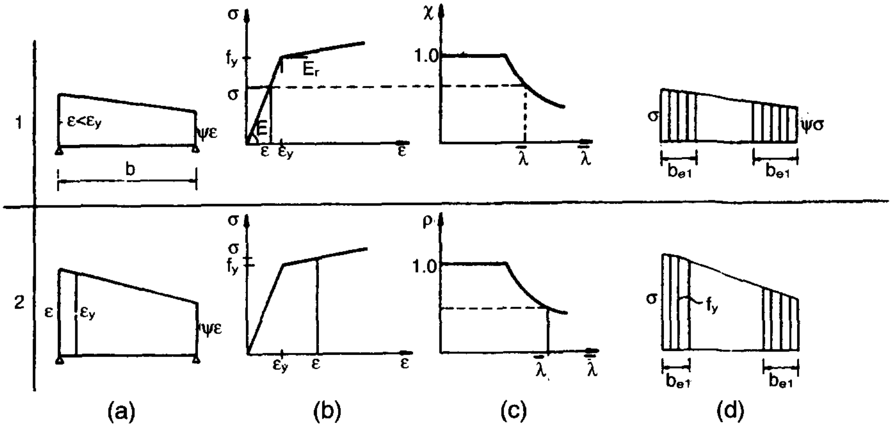

Fig. 5. Design methodology for plates: (a) strain distribution; (b) σ–ϵ characteristic; (c) buckling curve; (d) effective width.

is distributed along the supported edges according to the relevant specifications (e.g. Eurocode 3 [4]). Subsequently, the stresses are determined in accordance with the assumed σ–ϵ diagram, and the resulting axial force and bending moment of the plate panel may be evaluated by appropriate integration of the stresses within the effective width. The application of eqns (6)–(12) requires the selection of relations for the determination of σ_{cr} and χ. Evidently, σ_{cr} is equal to the critical plate buckling stress calculated from

$$\sigma_{cr} = k_\sigma \frac{\pi^2 E}{12(1-\nu^2)} \left(\frac{t}{b}\right)^2 \tag{13}$$

where k_σ is the buckling coefficient, ν is Poisson's ratio, and b and t are the width and thickness of the plate panel.

For plates, the Winter buckling curve given by

$$\chi = \frac{1}{\bar{\lambda}} - \frac{0.22}{\bar{\lambda}^2} \tag{14}$$

is usually applied. Geometrical imperfections and residual stresses are herewith globally taken into account. Fig. 6 shows the application of the method to plates with different boundary conditions subjected to compression. This figure shows how stresses above the yield stress, depending on the b/t ratios

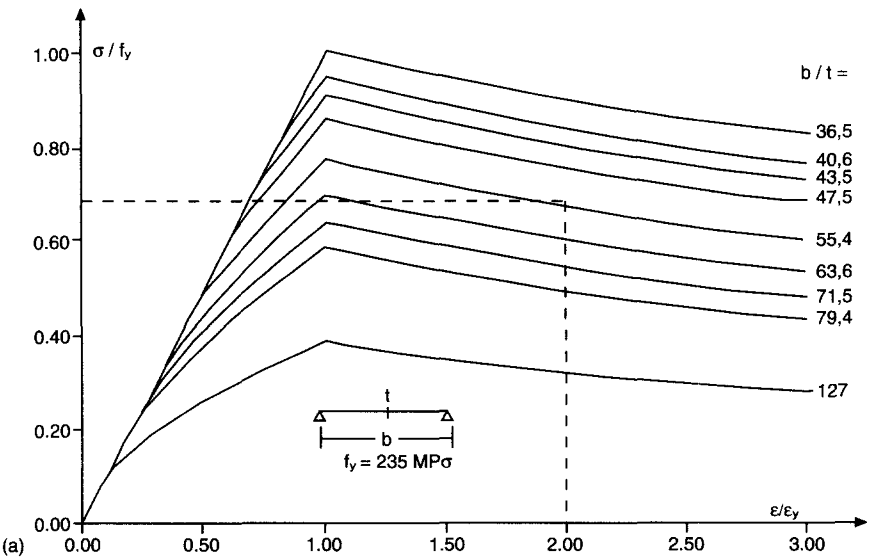

Fig. 6. Stress–strain diagrams of plates subjected to compression: (a) simple supported edges; (b) fixed edges.

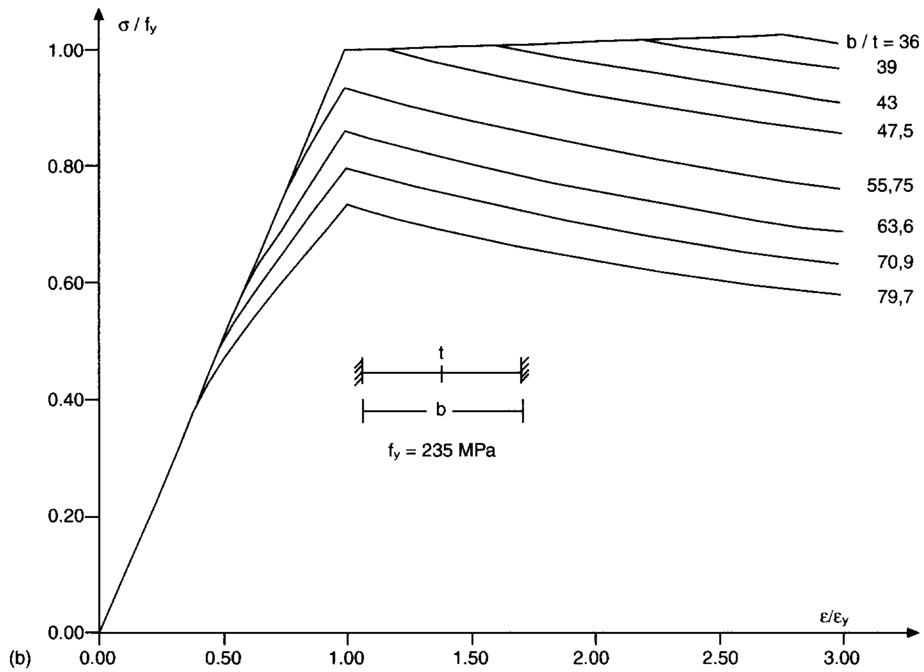

Fig. 6. Continued

and the supporting conditions, and how the response in the post-critical range may be evaluated. More specifically, Fig. 6(b) shows that, unlike the results of the conventional application of the effective width method, the limit stress may be achieved at strains larger than ϵ_y and may be due to strain hardening larger than the yield stress.

A more elaborate analysis is shown in Fig. 7, where geometrical imperfections and residual stresses are explicitly taken into account and may be performed by determination of the plate deflections at each loading level, a slight modification of the expression of the Winter curve, and consideration of the existing residual stresses over the plate width in the σ–ϵ diagram of each plate fibre. For more details in connection with the method, its applications and the comparison with other experimental results, reference is made to Vayas and Psycharis [6].

4 BEHAVIOUR OF CROSS-SECTIONS

A cross-section of any form may be thought of as consisting of individual plate panels supported along one or two edges (unstiffened or stiffened elements according to LRFD [3]). The behaviour of the section as expressed

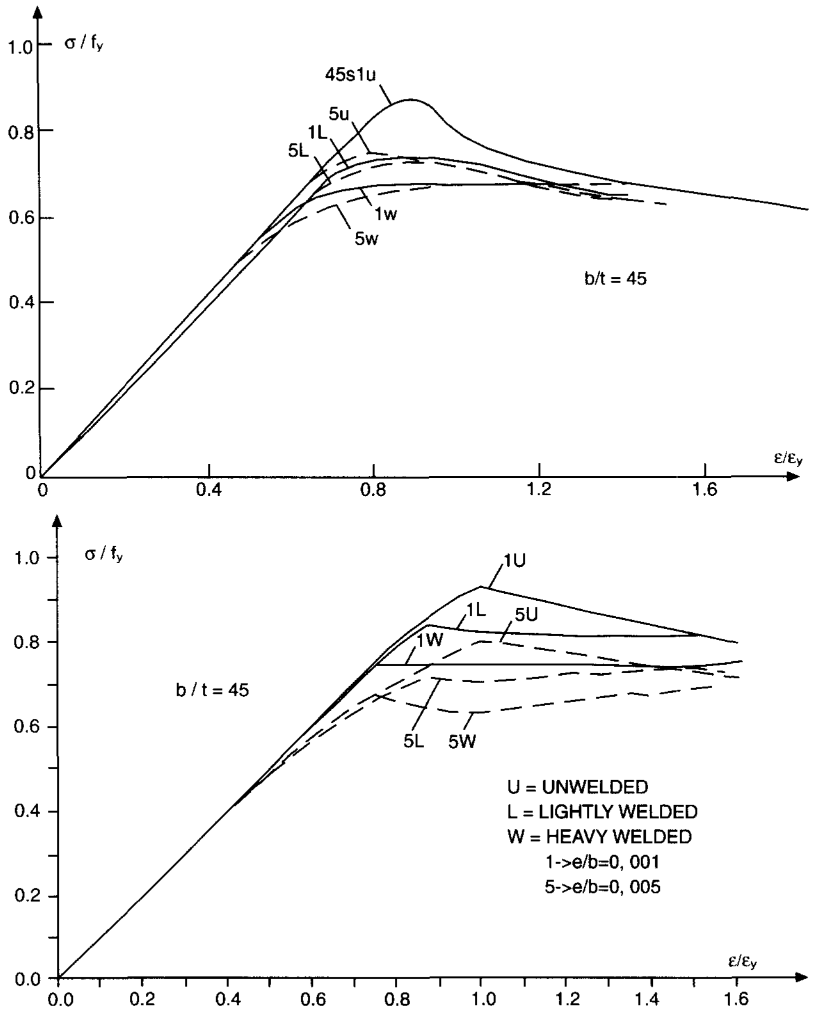

Fig. 7. Load-shortening curves for plates with imperfections according to (a) tests [8] and (b) the present method.

by stress–strain (σ–ϵ) or moment–curvature (M–k) curves depends on whether it is subjected to pure compression or to bending, without or with axial force. In both cases a strain-oriented formulation, like for plates, is required. Accordingly, a linear varying strain distribution over the cross-section is assumed, since plane sections shall remain plane (Fig. 8). This results in a certain strain distribution along the individual plate panels. For these panels the effective widths and stresses are determined. The resulting forces and moments are found by appropriate integration. Moment–curvature diagrams of cross-sections are shown in Fig. 9. For a more accurate description of the cross-sec-

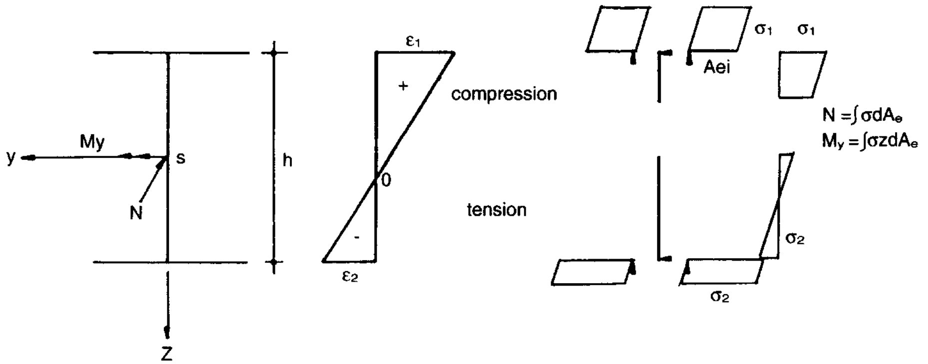

Fig. 8. Procedure for cross-sections.

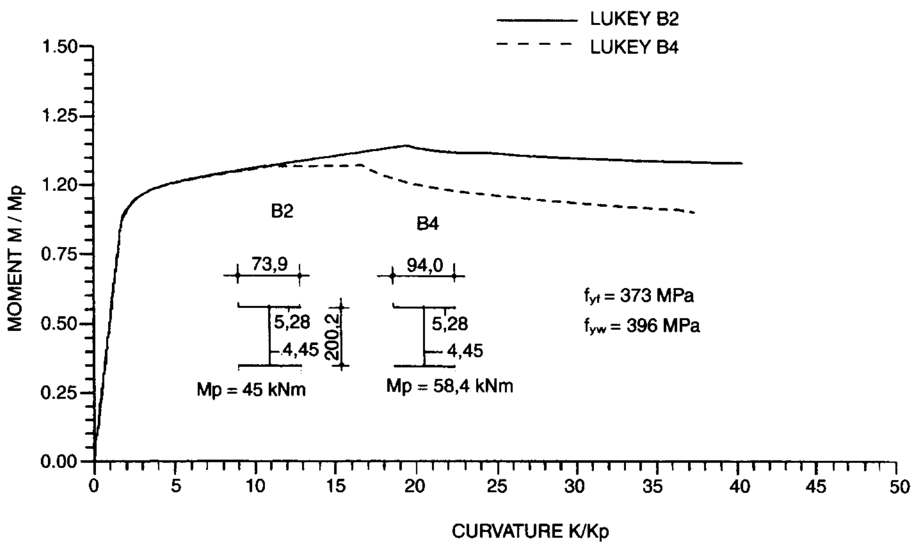

Fig. 9. Moment–curvature diagrams of sections with various flange slendernesses.

tional behaviour, rigid zones at element intersections and the partial restraint of flange buckling due to the web stiffness may be taken into account [9].

5 BEHAVIOUR OF BEAMS

The behaviour of beams subjected to transverse loads may be derived from the relevant M–k curves of the cross-section they are composed of. The procedure is shown for a simply supported beam subjected to a concentrated load at midspan (Fig. 10). This is a typical experimental arrangement for the determination of limiting *b/t* ratios for classification of cross-sections into categories, according to the relevant specifications (e.g. class 1, 2, 3 or 4 according to EC 3). The structural behaviour is represented by means of moment–rotation or moment–deflection curves. In order to derive analytically such curves both prior to and after the attainment of the ultimate load, a strain-oriented procedure such as in experimental investigations has to be applied. Accordingly, a certain curvature k_m at midspan is assumed. This corresponds, according to the M–k curve of the cross-section, to a moment M_m at midspan from which the moments, and hence the curvatures, over the entire beam may be calculated. The end rotation or midspan deflection of the beam are then determined by appropriate integration according to

$$\theta = \int M_1' \frac{M}{EI}\,\mathrm{d}x = \int M_1' k\,\mathrm{d}x \tag{15}$$

or

$$\delta = \int M_2' \frac{M}{EI}\,\mathrm{d}x = \int M_2' k\,\mathrm{d}x \tag{16}$$

where M denotes moments due to the actual load conditions and M_1' and M_2' denote moments due to the virtual unit moments and forces.

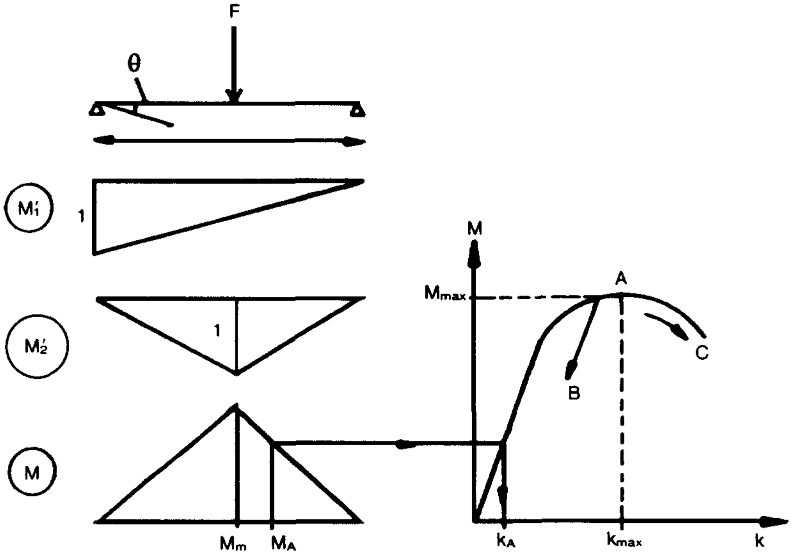

Fig. 10. Determination of moment–rotation or moment–deflection curves of simply supported beams.

The procedure is repeated until $k_m = k_{max}$, where the latter is the section curvature at maximum moment. Subsequently, the system becomes indeterminate since from one value of the applied moment two values of curvature, one smaller and one larger than k_{max}, may be determined. A solution is achieved if a plastification region at midspan, having a length l_p equal to the plastic hinge length, is assumed. The beam curvatures within that region are larger, outside it smaller than k_{max}. The calculation of the curvatures outside l_p becomes somewhat cumbersome, since the beam sections in these regions are subjected to unloading when the beam ultimate moment is reached (Fig. 10). It is therefore required to store the moment and curvature values of all sections outside the plastic hinge region in order to evaluate the unloading curve for each of them. This is obviously significant only for cross-sections where plastification during loading occurs. Otherwise, loading and unloading curves are identical. Experimental vs theoretical results for test girders are shown in Fig. 11. More detailed information on the procedure may be found in Vayas and Psycharis [9]. The proposed procedure was extensively applied by Wittemann [7] for the determination of rotational capacities of cold-formed members. The author made the remark that "the application of the method for the derivation of a

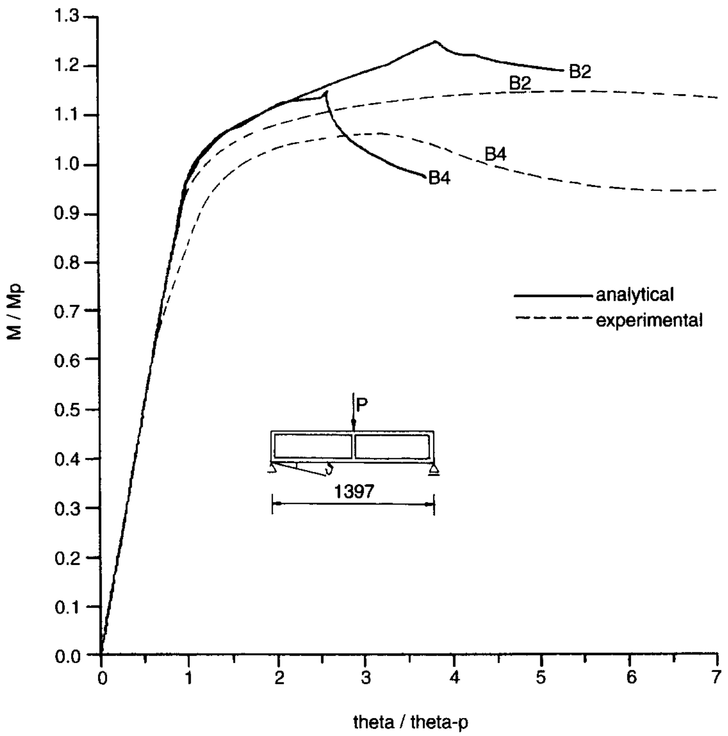

Fig. 11. Moment–rotation curves according to tests of Luckey [10] and the present method. Test girders as in Fig. 9.

complete moment–deflection-curve required 20 minutes computational time on a PC 486, while the corresponding computational effort using the Finite Element method was with all restarts a total of more days on a work station of the computer center of the University (of Karlsruhe)".

6 BEHAVIOUR OF COLUMNS

Axially compressed columns usually fail by global flexural buckling, local buckling or a combination of these buckling modes (rotation of the cross-sections restricted). Such columns may be treated, similarly to plates, by appropriate application of the strain-oriented method. According to the conventional design methods, local buckling is taken into account by calculating the columns with slender cross-section on the basis of the effective area, while for compact sections the gross area is used. The present method treats all classes of cross-sections equally, since local buckling may occur as stated before even in a compact section if it is subjected to large strains (eqns (6) and (9)). Accordingly, the column is supposed to be subjected to a specific axial strain ϵ for which the effective cross-section is determined by the procedures described in previous sections. Global buckling is then accounted for by determination of (a) the column slenderness according to eqn (6) or (9), where σ_{cr} is the Euler column stress, and (b) a reduction factor χ in accordance with the relevant column buckling curve (flexural, lateral torsional, etc.). More specifically, if a European buckling curve may be used, the relevant expression for the reduction factor is

$$\chi = \frac{1}{\phi + \sqrt{\phi^2 - \lambda^2}} \tag{17}$$

where

$$\phi = 0.5[1 + \alpha(\bar{\lambda} - 0.2) + \bar{\lambda}^2] \tag{18}$$

and α is the imperfection factor given as a function of the equivalent geometric imperfection.

Obviously the procedure is the same if any other expression of the reduction factor according to other codes is used.

The validity of the proposed method will be verified by comparison of its results with corresponding experimental ones. For that purpose the experimental investigations of Rieman *et al.* [11] will be used. The test specimen consist of a 7 mm plate panel longitudinally stiffened by four stiffeners (Fig.

12). The stiffeners have bulbed flat cross-section of type HP 140 × 7 (height 140 mm, thickness 7 mm, area 12.6 cm^2) according to the relevant German specifications. The parameters of the tests were the global column slenderness l/i (l = column length, i = radius of gyration of the gross cross-section) and the local plate slenderness b/t. The specimens were fabricated and thermally treated in a way to ensure that practically no geometrical imperfections or residual stresses were present, and are therefore considered as perfect. The notation of the specimen includes one letter and two figures. The letter indicates the type of imperfections – A stands for perfect models – while the figures indicate the values of the global and the local plate slendernesses (Table 1). Actually, these tests were intended to provide experimental data on the behaviour of axially loaded stiffened plates acting as flanges of bridge deck sections. However, due to the lack of longitudinal support, the models may be treated like compressed struts. This corresponds to densely stiffened flange plates where the actually existing longitudinal support has practically no influence on the carrying capacity. At this stage it should be clarified that the specific experiments, like those used in the following chapters, were selected as references for the proposed analytical method, since it was considered that they constitute the most complex cases of columns and beam columns, where various parameters interact very differently resulting in a large spectrum of different element behaviour and failure modes. It was therefore thought that an analytical method that is able to accurately predict the response of these tests is possibly suited for design purposes.

For the analytical simulation of the column behaviour, the general strain-oriented procedure described above was applied with the following specific features.

(1) Local buckling of the plate panels was taken into account by consideration of the Winter curve as buckling curve.
(2) Local buckling of the stiffeners was taken into account by application

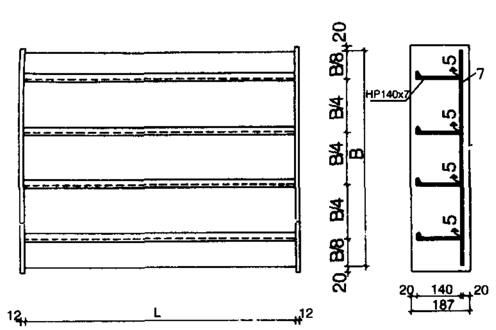

Fig. 12. Test specimen for columns and beam columns.

TABLE 1
Data for the Test Specimen

	All models				A models		D models		E models	
	b/t	l/i	l [mm]	B [mm]	f_y^a [MPa]	e_{max} [mm]	f_y^b [MPa]	e_{max} [mm]	f_y^b [MPa]	e_{max} [mm]
25–20	25	20	870	700	300	0	250	18.7	250	− 13.3
25–70	25	70	770	1400	298	0	254	16.4	249	− 13.6
25–100	25	100	680	2100	292	0	254	24.9	248	− 23.0
50–20	50	20	3530	700	309	0	248	16.7	249	− 16.5
50–70	50	70	3180	1400	306	0	256	18.1	248	− 14.5
50–100	50	100	2860	2100	259	0	256	26.6	248	− 21.3
75–20	75	20	5130	700	313	0	248	16.7	248	− 13.7
75–70	75	70	4630	1400	276	0	256	17.7	249	− 10.8
75–100	75	100	4170	2100	310	0	248	22.5	248	− 13.8

[a] The values of the table are weighted mean values, taking into account the relative areas of the plate panels and stiffeners. The individual values are as follows: stiffener web f_y = 268–282 MPa; stiffener bulb f_y = 265–275 MPa; plate panel f_y = 258–328 MPa.
[b] The same applies as for [a], the corresponding individual values are: stiffener web f_y = 260 MPa; stiffener bulb f_y = 278 MPa; plate panel f_y = 246–257 MPa.

of the European buckling curve ‘c’ for lateral torsional buckling, as described in the following sections.

(3) Global buckling was taken into account by application of a European buckling curve (eqn (17)) with a value of the imperfection parameter $\alpha = 0$, since the nine models under consideration were theoretically free from imperfections. However, as extensive geometric measurements on the models showed, it was not possible to fabricate a specimen of such dimensions without any geometric imperfections. The initial bow, e.g. under the four stiffeners, was generally different (Fig. 13(a)). The A models were therefore considered as free from imperfections in the sense of a ‘mean’ value (Table 1).

(4) The analysis was performed with measured mean values of the geometrical properties of the models (e.g. thickness of plate panels and stiffeners that generally differed from the nominal value of 7 mm). For steel, the upper and static yield stresses of the plate panels, the bulb and the web of the stiffeners for both tension and compression were available from measurements. For the analysis the measured weighted mean value of the upper tensile yield stress was used (Table 1).

The experimental vs theoretical results are shown in Fig. 14. The experimental ultimate loads and stresses are summarized in Table 2. Although the

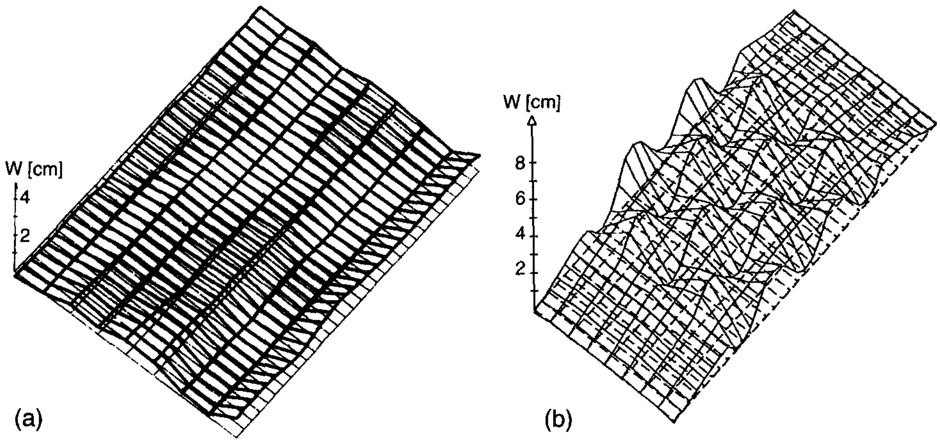

Fig. 13. Actual initial imperfections for (a) model A 75–70 and (b) model D 50–70.

general characteristics of all specimen are similar, the real structural behaviour is very different for the various models depending on the geometrical properties. The models with b/t = 25 have a compact cross-section so that global buckling is the governing failure mode. On the other side, models with b/t = 75 have a slender cross-section and fail primarily in the plate buckling mode. Models with l/i = 100 constitute slender struts where global buckling prevails, unlike the stocky models with l/i = 20 for which global buckling plays a secondary role. Regarding combinations of these parameters, it may be observed that model A 25–20 is a large coupon specimen, model A 25–100 fails in a pure global buckling mode, while model A 75–20 fails in a pure local plate buckling mode.

The general behaviour of all models as determined experimentally and theoretically is very much the same. The models behave linearly up to the attainment of the limit load due to the lack of imperfections. The failure is nonductile, even for the models (like A 75–20) that primarily fail in the plate buckling mode. In these models, however, the resistance is stabilized at large strains. Concerning the degree of approximation between analytical and experimental results, the following considerations shall be taken into account. In the present paper no proposal was made for a new resistance formula for members. This requires, as discussed before, extensive statistical evaluations with test results. The paper's intention is the description of the member behaviour beyond the limit load, adopting resistance formulae from design codes. These formulae were derived from such statistical evaluation of hundreds of tests. It is therefore expected that deviations between analytical and experimental results for the specific models examined occur here. Additional reasons for such discrepancies are discussed in the corresponding sections. For the present models it is observed that the analytically determined ultimate loads

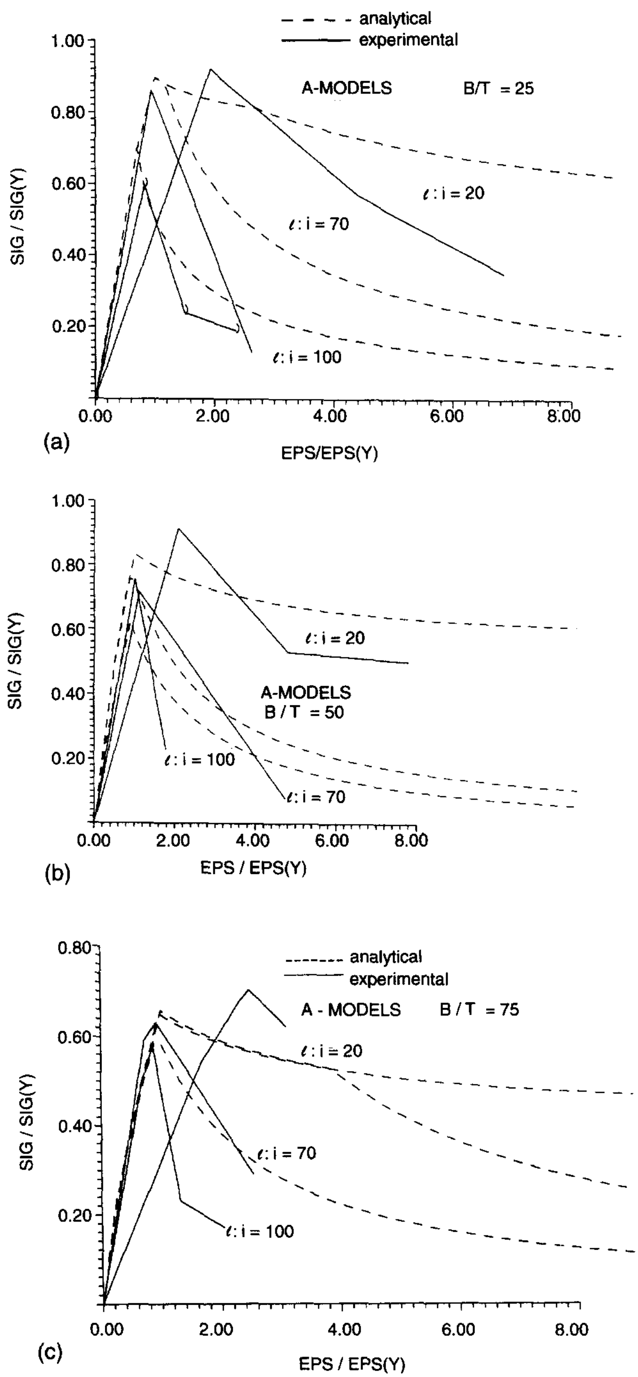

Fig. 14. Load-shortening curves for A models: (a) b/t = 25; (b) b/t = 50; (c) b/t = 75.

TABLE 2
Experimental Ultimate Loads and Ultimate Stresses

	A models		*D models*		*E models*	
	P_{max} *[kN]*	σ_{max} *[MPa]*	P_{max} *[kN]*	σ_{max} *[MPa]*	P_{max} *[kN]*	σ_{max} *[MPa]*
25–20	2808	276	1936	191	1880	185
25–70	2623	257	1430	141	1256	123
25–100	1756	174	972	96	836	82
50–20	4222	282	2131	143	2249	151
50–70	3264	219	1628	109	1447	96
50–100	2882	196	1182	79	985	66
75–20	4342	218	2491	126	2862	145
75–70	3495	174	1735	88	1591	80
75–100	3523	181	1309	66	1237	62

for the short models ($l/i = 20$) with large b/t (50 or 75) values are somewhat smaller than the corresponding experimental ones. This is due to the fact that the Winter curve was used for plate buckling. This curve is valid, as stated before, for plates with medium imperfections and is accordingly not able to accurately predict the response of the perfect plate panels considered here.

7 BEHAVIOUR OF BEAM COLUMNS

Stiffened plates like those examined in the previous section may generally fail in two possible modes of failure:

- plate failure caused by plate buckling, where the deformations at failure consist of a global, overall deflection towards the stiffener and local buckling of the plate panel between the stiffeners (Fig. 15(a)); and
- stiffener failure caused by lateral torsional buckling of the stiffeners, where the deformations at failure consist of a global, overall deflection towards the plate and local buckling of the stiffeners (Fig. 15(b)).

For the study of the behaviour of imperfect stiffened plates, further tests on two series of models having the same overall dimensions as presented before, but with imposed imperfections, were carried out [12]. Models D had global and local geometrical imperfections that led to plate failure, while the imperfections of models E led to stiffener failure. The values of these imperfections corresponded nominally to four times the values prescribed by the MERRISON Report [13]. The actual values of the global imperfections for

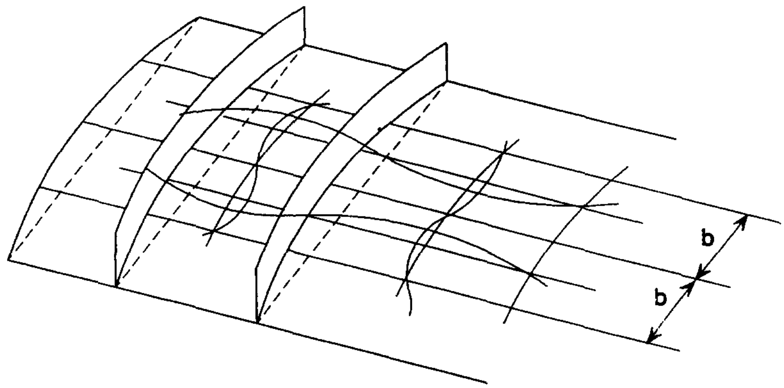

(a)

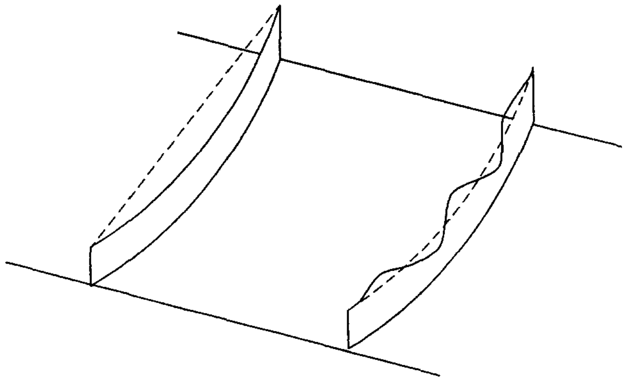

(b)

Fig. 15. Failure modes and deformations at failure of stiffened plates: (a) plate and (b) stiffener failure.

the two test series, which as will be seen later are taken explicitly into account in the calculations, are shown in Table 1. In addition to the global imperfections, local imperfections were imposed on the specimen. Models D had local plate imperfections in a checkerboard, or 'hungry horse', pattern with a half-wavelength equal to the distance b of the stiffeners and an amplitude f_{pl} (Fig. 13(b) and 15(a)). Models E had local stiffener imperfections with a half-wavelength equal to 290 mm and an amplitude at the bulb equal to f_{st} (Fig. 15(b)). The imperfections were imposed only in the central part of the models where failure was expected to occur. The actual mean and maximal values of the local imperfections as well as the number of half-waves in the longitudinal direction are summarized in Table 3. In both series, residual welding stresses were also present. In order to accurately simulate the experimental behaviour, two separate types of analysis in correspondence to the two modes of failure were needed.

7.1 Interaction of global buckling with plate buckling

The present analysis refers to the simulation of the behaviour of models D whose imperfections lead to plate failure. In principle, two alternative design methods may be applied. The models may be analytically treated:

- as axially compressed columns with a geometrical overall imperfection; or
- as beam columns subjected to axial compression and transverse bending.

Both idealizations will be presented and discussed subsequently. If the models are treated as axially compressed columns with a global geometrical imperfection, the design formulae that have already been presented for columns (eqns (17) and (18)) are to be applied. The imperfection factor α may be calculated from the global geometrical imperfection. The relevant relation proposed by Eurocode 3 is written as

$$\alpha(\bar{\lambda} - 0.2)W/A = e \tag{19}$$

TABLE 3
Actual Values and Number of Local Imperfections in Longitudinal Direction

	D models			*E models*		
	f_{pl} *[mm] mean*	f_{pl} *[mm] max*	N	f_{st} *[mm] mean*	f_{st} *[mm] max*	N
25–20	4.3	5.3	4	3.2	3.7	1
25–70	4.4	5.6	7	3.2	4.5	9
25–100	3.9	7.2	7	3.3	5.9	15
50–20	8.8	9.7	1	3.1	3.4	1
50–70	9.2	14.7	5	3.4	4.2	9
50–100	8.7	12.1	7	3.3	5.2	13
75–20	10.4	15.5	1	2.7	3.7	1
75–70	13.3	15.9	3	5.5	6.2	7
75–100	12.3	15.9	5	5.4	7.2	11

where W is the section modulus, A is the cross-sectional area, and e is the value of the global imperfection.

The application of this procedure did not lead to satisfactory results, especially where the post-ultimate behaviour of the short models was concerned, for reasons to be explained later. The treatment of the models as beam columns therefore seemed more appropriate. For that purpose the limit state equation of a torsionally restrained column subjected to axial forces and bending moments shall be taken into account. Such an equation can be adopted from any design code. In the context of the present paper the relevant expression of Eurocode 3 is considered:

$$\frac{N_{Sd}}{\chi A f_y} + \frac{k M_{Sd}}{W f_y} = 1 \tag{20}$$

where N_{Sd} = applied axial load, M_{Sd} = bending moment due to imperfection and shift of the neutral axis, χ = reduction factor for column buckling (eqn (17)).

$$k = 1 - \frac{\mu N_{Sd}}{\chi A f_y} < 1.5 \tag{21}$$

$$\bar{\mu} = \bar{\lambda}(2\beta - 4) + (\alpha_{pl} - 1) \leq 0.9 \tag{22}$$

where α_{pl} = shape factor for the cross-section, $\beta = 1.3$ for the bending moment distribution under consideration, A, W = area and modulus of cross-section appropriately reduced due to local buckling.

As in the previous sections, a strain-oriented procedure has to be applied requiring a reformulation of the limit state equation (20), in order to investigate the element behaviour beyond the limit load. For that purpose a compressive strain ϵ is applied and the reduction factors for local plate buckling (eqn (14)), referring to the plate panel that is primarily in the compression zone, and global buckling (eqn (17)) are calculated. The structural response is found from the expression

$$\frac{\sigma}{f_y} = \left(\frac{1}{\chi n} + \frac{ke}{W_e \sigma_0 / A f_y}\right)^{-1} \tag{23}$$

where χ is the reduction factor for global buckling according to eqn (17) with $\alpha = 0$ since global imperfections are explicitly taken into account by the limit state equation

$$n = A_e \sigma_0 / A f_y$$

where A and A_e are the gross and effective area of the cross-section, σ_0 is the stress that corresponds to the applied strain ϵ according to the material law, W_e is the modulus of the effective cross-section, and $k = 1 - (\mu/\chi)n \leq 1.5$.

The experimental vs theoretical results are shown in Fig. 16. The analytical results are generally in good agreement with the experimental ones, especially in the post-ultimate range taking into account the complexity of the problem and the large number of influencing factors. It should be emphasized that for a more accurate description of the experimental behaviour the complete set of mechanical and geometrical properties of the test specimen should be included. This would require more elaborate analysis, like the application of finite elements. The efficiency of a design model such as the one proposed here should, however, be checked against experimental results in the sense described in the Introduction of the present paper. The most remarkable discrepancy between experimental and theoretical results is observed in the initial stiffness of the models. The experimental curves provide, due to the large local geometrical imperfections, lower initial stiffness than that corresponding to the slope of the elastic line $\sigma = \epsilon E$. This 'accordion' effect is, however, not included in the analysis, where local buckling is globally taken into account by the Winter curve which yields elastic behaviour at small strains.

The model response is influenced by three factors, i.e. bending, local buckling and global buckling. Bending and local plate buckling provide ductile modes of failure, while failure due to global buckling is rather brittle as shown in the previous section. The overall behaviour of the D models is very ductile, which shows that bending and local plate buckling have a dominating influence on the failure mechanism. This explains that short models ($l/i = 20$), in which global buckling plays an inferior role, have the most ductile behaviour. For a correct prediction of the structural behaviour, all modes of failure should be explicitly included in the limit state equation. From the two alternative procedures presented at the beginning of the section, only the second includes explicitly the three influencing factors. The first procedure includes the effects of bending indirectly through the imperfection parameter α, so that it possesses the main features of global buckling where the type of failure is concerned. This is the reason why the corresponding results were not satisfactory, especially beyond the limit load, and the method was withdrawn. Finally, it may be observed that the ultimate loads of the D models are lower than the corresponding loads of the perfect A models. At higher strains, however, D models possess higher strength than perfect A models. This observation may be useful for the definition of alternative design criteria in future codes.

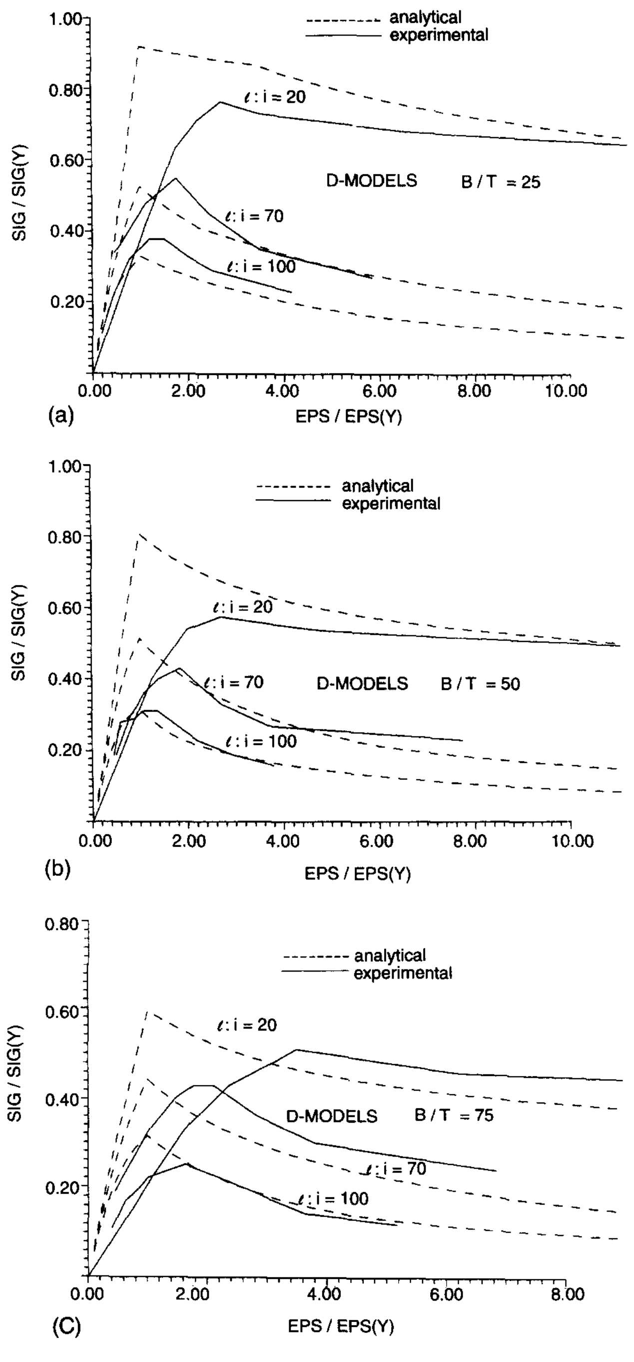

Fig. 16. Load-shortening curves for D models: (a) b/t = 25; (b) b/t = 50; (c) b/t = 75.

7.2 Interaction of global buckling with lateral torsional buckling

The current analysis refers to the simulation of the E models whose imperfections lead to stiffener failure as explained before. The values of the maximum imperfections at midspan and the material properties are shown in Table 1. The analytical treatment of these models is similar to that of the D models. The limit state expression is the same as before (eqn (23)). The two analyses differ, however, in the determination of the effective area of the cross-section, i.e. the way in which local buckling is accounted for. The stiffeners in the E models are in the compression zone and fail by lateral torsional buckling since they rotate around the plate. This is taken into account by using the buckling curve for lateral torsional buckling in the computation of the effective area of the stiffener, while the effective area of the plate panel is determined on the basis of lower stress as a result of the global imperfection. According to the provisions of Eurocode 3, the buckling curve for lateral torsional buckling is identical with the global buckling curve (eqn (17)) with the exception that it starts to decrease at values of slenderness $\bar{\lambda} > 0.4$ (Fig. 12).

The experimental vs theoretical results are shown in Fig. 17. Again, a good agreement between experimental and theoretical results in all ranges of behaviour is achieved. The failure mechanism is in this case nonductile. The reason is that in these models local buckling, which is caused by lateral torsional buckling, leads in combination with global buckling to brittle types of failure. This is expressed analytically by the use of a global buckling curve for the case of lateral torsional buckling, which is rapidly decreasing for increasing slenderness leading therefore to nonductile failure.

8 CONCLUSIONS

A design model for the simulation of the behaviour of steel structural elements beyond their ultimate load was presented. The method is based on a strain-oriented formulation of the expressions used for the solution of stability problems. It may equally be applied to various problems that are associated with different types of instability. A wide range of applications where failure is initiated by local plate buckling, global column buckling or lateral torsional buckling was shown. The applications include individual compressed plate panels, beams subjected to transverse bending, columns subjected to axial compression, and beam columns in the form of compressed stiffened plates with imperfections. The analytical results were compared with corresponding experimental ones. The comparisons showed that the proposed method is well suited for application to stability problems. For the elements investigated, several types of failure with different characteristics with respect to ductility were

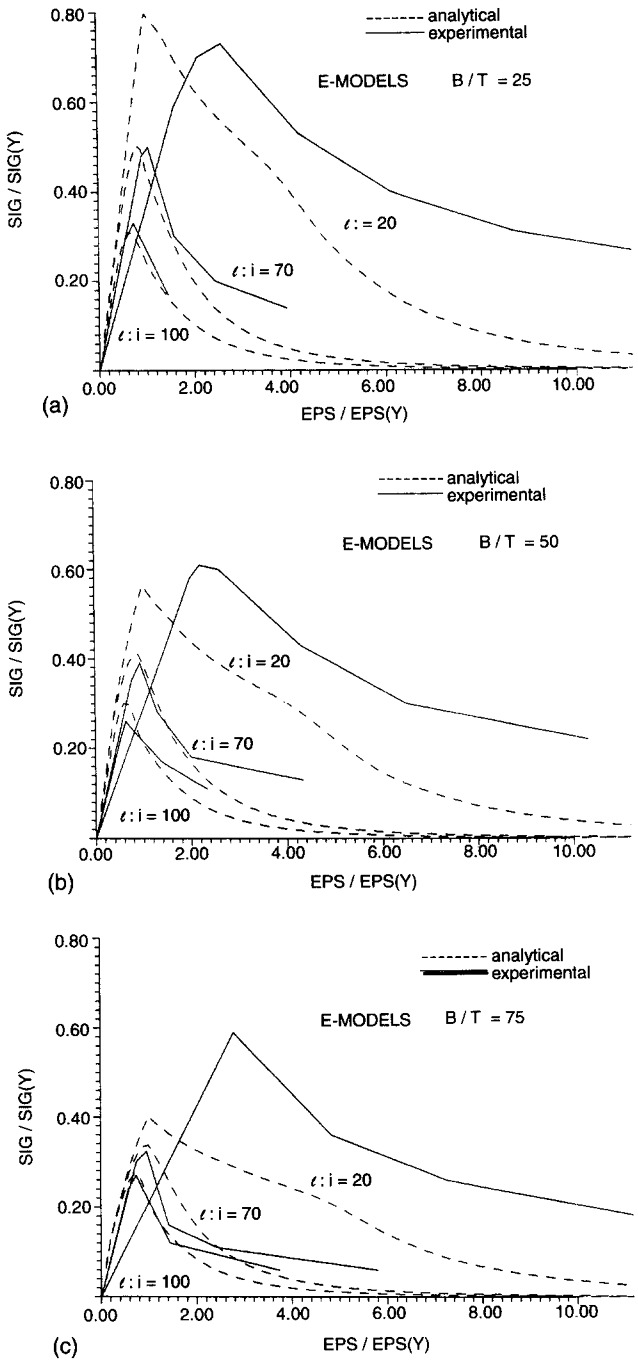

Fig. 17. Load-shortening curves for E models: (a) $b/t = 25$; (b) $b/t = 50$; (c) $b/t = 75$.

detected. Failure is ductile if bending or local plate buckling are the prevailing failure modes, while global column buckling or lateral torsional buckling lead to nonductile failure. The proposed method may serve as a basis for direct ductility evaluations of steel structural elements. This might enable a reformulation of the relevant criteria included in the present design codes through a direct comparison between required and available ductility.

REFERENCES

1. British Standard 449, The use of structural steel in building, 1939.
2. DIN 1050, Stahl im Hochbau, Berechnungsgrundlagen für Stahlbauten, 1936.
3. Load and Resistance Factor Design LRFD, Specification for structural steel buildings. AISC, 1986.
4. Eurocode 3, Design of steel structures. CEN, European Committee for Standardization, ENV 1993-1-1.
5. Eurocode 3, Annex Z, Determination of design resistances from tests. CEN, European Committee for Standardization, ENV 1993.
6. Vayas, I. and Psycharis, I., Dehnungsorientierte Formulierung der Methode der Wirksamen Breite. *Stahlbau*, 1992, **61**, 275–283.
7. Wittemann, K., Traglastermittlung für Kaltprofile. Ph.D. thesis, TH Karlsruhe, Germany, 1993.
8. Bradfield, C. D., Tests on plates loaded in in-plane compression. *Journal of Construction Steel Research*, 1980, **1**, 27–37.
9. Vayas, I. and Psycharis, I., Ein dehnungsorientiertes Verfahren zur Ermittlung der Duktilität von Trägern aus I-Profilen. *Stahlbau*, 1993, **62**, 333–341.
10. Luckey, A. F. and Adams, P. F., Rotation capacity of beams under moment gradient. *Journal of Structural Division*, 1969, **95**, 1003–1023.
11. Rieman, S., Schmidt, H. and Barbre, R., Versuche an 9 durch Wulstflachstähle längs versteiften Blechfeldern ohne geometrische Imperfektionen und ohne Eigenspannungen. Bericht 7201-2 B des Instituts für Stahlbau der TU Braunschweig, 1976.
12. Rieman, S., Schmidt, H. and Barbre, R., Versuche an 18 durch Wulstflachstähle längs versteiften Blechfeldern mit geometrischen Imperfektionen und Eigenspannungen. Bericht 7201-4 B des Instituts für Stahlbau der TU Braunschweig, 1976.
13. Inquiry into the basis of design and method of erection of steel box girder bridges. Report of the Committee (MERRISON-Report), Appendix 1: interim design and workmanship rules. HMSO, London, 1973.